SEMARAK ILMU PUBLISHING

Journal of Advanced Research in Fluid Mechanics and Thermal Sciences

Journal homepage:
https://semarakilmu.com.my/journals/index.php/fluid_mechanics_thermal_sciences/index
ISSN: 2289-7879

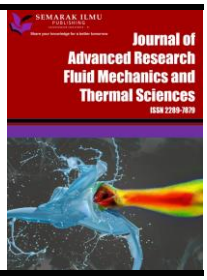

Analysis of Nanofluid Flow Over a Heated Circular Cylinder using the Volume of Fluid (VOF) Approach

Liyes Aguedal[1,*], Rachid Bessaïh[1]

[1] Department of Mechanical Engineering, LEAP Laboratory, University of Mentouri Brothers-Constantine 1, Constantine, 25000, Algeria

ARTICLE INFO

Article history:
Received 17 July 2024
Received in revised form 29 October 2024
Accepted 12 November 2024
Available online 30 November 2024

Keywords:
Nanofluid; circular cylinder; two-phase approach; Volume of Fluid (VOF); heat transfer; vortex shedding

ABSTRACT

This study employs a two-phase Volume of Fluid (VOF) model to investigate the flow and heat transfer characteristics of Al_2O_3-water nanofluid over a heated circular cylinder at a Reynolds number of 100. Nanoparticle volume fractions (Φ) ranging from 1% to 10% were analyzed. A comprehensive grid-independence study and code validation were conducted to ensure the accuracy of the results. Increasing (Φ) from 0% to 10% led to significant changes in flow parameters: the mean drag coefficient increased by 27.8% (from 1.33 to 1.7), the fluctuating lift coefficient rose by 56.5% (from 0.23 to 0.36), and the Strouhal number increased by 6.7% (from 0.164 to 0.175). Heat transfer enhancement was observed with increasing nanoparticle concentration, as evidenced by the local Nusselt number at the front stagnation point (θ = 0°) rising by approximately 40% over the same (Φ) range. The study revealed significant changes in pressure distribution around the cylinder, with higher (Φ) values smoothing the pressure gradient and altering the separation point. Time-averaged temperature contours demonstrated more uniform thermal distributions and reduced wake sizes at higher (Φ) values, indicating improved thermal diffusion and heat transfer efficiency. The (VOF) model successfully captured complex two-phase flow dynamics, revealing asymmetric nanoparticle distributions in the wake region at higher concentrations. These findings have important applications in thermal management systems, including electronic and energy systems, potentially leading to more efficient cooling systems and heat exchangers.

1. Introduction

In recent years, research on nanofluids has gained considerable attention. These fluids possess much better thermophysical properties than conventional fluids. Nanofluids exhibit improved thermal conductivity as mixtures of nanoparticles and base fluids, making them highly attractive for various heat transfer applications.

Nanofluids can enhance thermal management systems, such as those used in electronic cooling, automotive industries, and energy systems. Traditional single-phase models frequently do not accurately capture the complex interplay between nanoparticles and base fluid. However, the two-

* *Corresponding author.*
E-mail address: liyes.aguedal@umc.edu.dz

https://doi.org/10.37934/arfmts.124.2.7189

phase approach offers a more comprehensive framework by treating the nanoparticles and the fluid as separate but interacting phases. This approach provides a deeper understanding of flow dynamics, heat transfer properties, and the influence of various parameters on the system's overall performance.

Safaei *et al.,* [1] review recent advancements in the mathematical modeling of nanofluids; they highlight the challenges associated with the experimental study of nanofluids, including high costs and difficulties in maintaining stable nanofluid suspensions, making computational fluid dynamics (CFD) emerges as a valuable tool for research. The review discusses various (CFD) approaches. They aim to identify the most effective simulation methods to enhance the application of nanofluids in energy devices, thus contributing to the optimization of thermal systems. Safaei *et al.,* [1] underscore the importance of two-phase models in the mathematical simulation of nanofluids. Unlike single-phase models, while models treating nanofluids as homogeneous mixtures simplify the analysis, two-phase models account for the unique behaviors exhibited by nanoparticles and the base fluid. This distinction is critical as it provides a more precise representation of fluid interactions and dynamics.

Using numerical simulations and experimental analysis, Naphon and Nakharintr [2] examine nanofluids' turbulent flow and heat transfer properties in minichannel heat sinks. They aimed to compare the effectiveness of different models, including the single-phase, mixture two-phase, and Volume of Fluid (VOF) approaches, in predicting the behavior of nanofluids. Their experimental setup involved a copper minichannel heat sink and a cooling system with TiO_2 nanoparticles, measuring parameters like flow rates and temperatures. They found that the mixture of two-phase and (VOF) models provided more accurate predictions than the single-phase model and that nanofluids significantly enhanced heat transfer compared to deionized water. Their investigation revealed that two-phase models, particularly (VOF) models and the mixture approaches, are better suited for examining the heat transfer of nanofluids in turbulent flows.

Abdelhamid *et al.,* [3] observed the impact of the Reynolds number (Re) and corner radius ratio (r/R) on the flow characteristics, aerodynamic forces, and heat transfer properties surrounding a square cylinder. They look at Reynolds numbers between 40 and 180 and corner radius ratios between 0.0 and 1.0. According to their findings, the critical Reynolds number for the start of vortex shedding decreases from 49.5 to 46.75 as the corner radius ratio rises, indicating that a larger corner radius encourages earlier vortex shedding. Unsteady trailing-edge separated flow, unsteady separation-bubble flow, unsteady leading-edge flow, and steady trailing-edge separated flow are the four different flow patterns found. The mutual influence of (r/R) and (Re) shapes these patterns. The research indicates that (r/R) and (Re) substantially influence the Strouhal number, which increases with these parameters, indicating enhanced heat transfer. Aerodynamic forces show a more pronounced sensitivity to (Re) than to (r/R), with complex dependencies on these variables. Additionally, Abdelhamid *et al.,* [3] examine variations in boundary layer thickness, shear layer velocity, and wake structure. They find that the maximum velocity within the shear layer rises with both (r/R) and (Re), whereas the thickness of the boundary layer decreases.

Park *et al.,* [4] numerically simulated a flow over a circular cylinder with Reynolds numbers (Re) up to 160 in high resolution, offering comprehensive information on flow quantities. Utilizing a non-uniform mesh with 641×641 points, the study solves the incompressible flow in a C-grid system through a fully implicit method. Key findings include the excellent agreement of the Strouhal number (St) with experimental data, the onset of vortex shedding at Re = 47, and alignment of mean pressure coefficient distribution with previous studies at Re < 45. As the Reynolds number increases, the overall drag coefficient decreases, while pressure drag becomes more significant in unsteady flow, and lift fluctuations are higher than drag fluctuations. The mean separation angle and its fluctuations increase with Re, and the length of the time-averaged separation bubble shows fair agreement with

past experiments. The study offers valuable data for validating experimental measurements and understanding flow physics at low Reynolds numbers, supporting the accuracy of the computational approach and providing insights into the effects of vortex shedding on drag and lift forces.

Nashee and Hmood [5] investigate air's thermal and flow characteristics over a circular cylinder, focusing on Reynolds numbers ranging from 100 to 5000. They employed FLUENT 19 software to solve governing equations. The analysis shows good agreement with previous research for the Nusselt number and a decrease in the drag coefficient with increasing Reynolds numbers. This research extends the numerical analysis to explore the Nusselt number, drag coefficient, and local pressure coefficient behavior. The 2D model, chosen for its large length-to-diameter ratio, utilized an unstructured mesh with grid independence verified using four different meshes. Results indicated an 11% deviation in Nusselt number values from previous studies for Reynolds numbers 100 and 1000, attributed to differing dimensional values and parameters. The study found that the drag coefficient decreases inversely with Reynolds numbers due to circulation zones. Maximum pressure occurs on the cylinder's front face, with a drop at the sides due to flow acceleration and boundary layer separation. Higher Reynolds numbers showed unstable, separated shear layers forming vortices, increasing heat transfer.

Bhattacharyya *et al.,* [6] conducted a numerical investigation into the heat transfer characteristics around a hexagonal cylinder placed in a channel. The study considered Reynolds numbers ranging from 100 to 50,000 and turbulence intensities between 5% and 50%, using air as the working fluid with a constant Prandtl number. They employed a three-dimensional model and used a grid with 22 542 nodes were generated through the Richardson extrapolation method. The simulations, carried out using Fluent 16.2, revealed that the average Nusselt number increases with both Reynolds and turbulence intensity, with a significant rise observed beyond a Reynolds number of 10,000. The transition from laminar to turbulent flow was identified around a Reynolds number of 2000, with detailed analyses of velocity vectors, temperature contours, and turbulent kinetic energy illustrating the complex flow patterns and heat transfer behavior. Bhattacharyya *et al.,* [6] concluded that the Shear Stress Transport (SST) model effectively predicts heat transfer across different flow regimes, providing a robust foundation for Computational Fluid Dynamics (CFD) simulations in more complex geometries, with results aligning well with empirical correlations.

Aun *et al.,* [7] explored the impact of low concentrations of diamond water nanofluid on the performance of loop heat pipes (LHPs). Their study focused on three mass concentrations of diamond nanofluid: 0.3%, 0.6%, and 0.9%, and evaluated the effects under varying flow rates and heat loads. The findings revealed that even at these low concentrations, diamond water nanofluid significantly enhances the heat transfer coefficient compared to pure water due to its superior thermal conductivity. Additionally, using diamond nanofluid reduced the total thermal resistance of the (LHP), indicating more efficient heat transfer. Notably, forming smaller bubbles in the vapor line with diamond nanofluid further contributed to better heat transfer characteristics. The experimental results were validated with ANSYS simulations, showing good agreement with less than 5% error between simulated and experimental temperatures. Aun *et al.,* [7] concluded that low concentrations of diamond water nanofluid could effectively improve the cooling performance of Loop Heat Pipes (LHPs), presenting a cost-effective alternative to higher-concentration nanofluids.

Majdi *et al.,* [8] examined natural convection within a wavy enclosure containing an inner circular cylinder. Using a finite element scheme, they analyzed the space filled with two layers: one with silver (Ag) nanofluid and the other with a porous medium saturated with the same nanofluid. They developed dimensionless equations for heat transfer and fluid flow and utilized the Darcy-Brinkman model to account for porous media. Key parameters investigated by Majdi *et al.,* [8] included the Rayleigh number (Ra), Darcy number (Da), cylinder radius (R), cylinder vertical position (δ), number

of undulations (N), and nanoparticle volume fraction (Φ). They found that increasing Ra, Da, and the volume fraction of nanofluid improves both fluid flow robustness and heat transfer efficiency. The optimal heat transfer was observed when the internal cylinder (R=0.2) was positioned vertically downward (δ=-0.2) with one undulation (N=1). Their findings, presented through streamlines, isotherms, and Nusselt numbers, highlight the significant impact of varying these parameters on heat transfer efficiency. In conclusion, Majdi *et al.,* [8] provided valuable insights into the influence of geometric and physical parameters on natural convection in nanofluid-filled wavy enclosures, offering guidelines for optimizing heat transfer performance in such systems. Several other studies have also investigated various aspects of non-Newtonian nanofluids in wavy geometries. Ahmed *et al.,* [9] studied forced convection of non-Newtonian nanofluid in a sinusoidal wavy channel, employing response surface analysis and sensitivity testing. Hossain and Molla [10] examined MHD mixed convection of non-Newtonian power-law ferrofluid in a wavy enclosure. In another study, Hossain *et al.,* [11] investigated MHD mixed convection of non-Newtonian Bingham nanofluid in a wavy enclosure with temperature-dependent thermophysical properties, using sensitivity analysis by response surface methodology. Afsana *et al.,* [12] explored MHD natural convection and entropy generation of non-Newtonian ferrofluid in a wavy enclosure. Additionally, Nag and Molla [13] studied double-diffusive natural convection of non-Newtonian nanofluid considering thermal dispersion of nanoparticles in a vertical wavy enclosure.

Using numerical simulations, Korib *et al.,* [14] analyzed the Cu-water nanofluid's flow characteristics and heat transfer over a circular cylinder. Within uniform heat flux (UHF) and constant wall temperature (CWT) parameters, they examined the steady flow-field and heat transfer for nanoparticle volume fractions ranging from 0% to 5% and Reynolds numbers between 10 and 40. In the study, a 2D infinitely long circular cylinder is modeled with uniform nanoparticles flowing at the base fluid's velocity while in thermal equilibrium. Equations relating to momentum and energy control the flow, which have particular velocity and temperature boundary conditions. A steady, laminar solver using the SIMPLE algorithm is employed. Results validate the numerical methods and show that higher Reynolds numbers lead to recirculation bubbles in nanofluids slightly displaced from the cylinder surface. Enhanced thermal conductivity of nanofluids results in higher local Nusselt numbers, improving heat transfer efficiency.

Mahat *et al.,* [15] investigate the behavior of viscoelastic nanofluids under the influence of a magnetic field. The study aims to understand how factors such as magnetic field strength, nanoparticle volume fraction, and fluid properties, including viscosity and thermal conductivity, affect the velocity, temperature, skin friction, and heat transfer coefficients as the fluid flows past a circular cylinder with constant heat flux. The researchers developed a mathematical framework using the Tiwari and Das nanofluid model. They employed the Keller box method to solve the dimensionless governing equations derived from the momentum and energy equations. The findings reveal that the magnetic field significantly influences the nanofluid's flow dynamics and heat transfer properties. Specifically, the fluid's velocity decreases as the magnetic field strength increases due to the Lorentz force, which acts as a drag on the fluid. Conversely, the temperature of the fluid rises with an increase in both magnetic field strength and nanoparticle volume fraction, enhancing the fluid's thermal conductivity. Additionally, the study found that skin friction increases with stronger magnetic fields and higher nanoparticle concentrations, while the heat transfer coefficient decreases as the magnetic parameter increases. These findings are consistent with previous studies, which highlight the critical roles that magnetic parameters and nanoparticle volume fractions play in modifying viscoelastic nanofluids' flow and thermal properties, with important implications for enhancing heat transfer in various industrial applications [16-37].

Urmi *et al.,* [38] examine the various types of nanofluids, their preparation methods, and their thermophysical properties, focusing on thermal conductivity and viscosity. The study highlights the widespread use of the two-stage method for preparing nanofluids and the ongoing research to achieve stable nanofluids with high thermal conductivity and low viscosity. The review notes that increased solid concentration of nanoparticles generally enhances thermal conductivity, with the highest improvement reported being 300% for kerosene-based oleic acid-coated Fe_3O_4 nanofluids. Viscosity, a crucial factor in heat transfer applications, typically increases with higher particle concentration and decreases with higher temperatures, with a maximum reported increase of 320% for water-based nanofluids with single-walled carbon nanotubes. Despite the novel properties of nanofluids, their industrial applications remain limited, necessitating further research. Future studies should investigate nanoparticle shape, synthesis methods, surfactant types, and ultrasonication times. The review underscores the need for large-scale experiments and comparative studies to advance the practical application of nanofluids in thermal engineering. This comprehensive review aims to guide the development of innovative nanofluids with improved properties for efficient thermal management solutions.

In recent years, the study of nanofluids has garnered significant attention due to their superior thermal properties compared to conventional fluids. Nanofluids, a mixture of nanoparticles and base fluids, exhibit enhanced thermal conductivity, making them attractive for heat transfer applications such as electronic cooling, automotive industries, and energy systems. While much research has been conducted on nanofluids, especially using single-phase models, there remains a gap in understanding the complex interactions between nanoparticles and base fluids in specific flow conditions. Many previous studies, such as those by Safaei *et al.,* [1] and Naphon and Nakharintr [2], highlight the limitations of single-phase models, which often oversimplify these interactions. Two-phase models, such as the Volume of Fluid (VOF) approach, offer a more accurate representation by treating the nanoparticles and base fluid as separate but interacting phases. Despite advancements, there is still a need for detailed studies on nanofluid behavior around specific geometries, such as circular cylinders, which are common in thermal management systems. This study aims to address these gaps by employing the (VOF) model to investigate the flow and heat transfer characteristics of Al_2O_3-water nanofluid over a heated circular cylinder. By examining the effects of varying nanoparticle volume fractions on flow parameters such as drag and lift coefficients, Strouhal number, and heat transfer rates, this research seeks to provide a deeper understanding of nanofluid dynamics.

2. Numerical Method

2.1 Mathematical Formulation

The (VOF) model uses a single momentum equation for each phase, solving a continuity equation for the secondary phases to track their volume fractions over the study domain. The volume fraction of the primary phase can be computed since the volume fractions of all the phases sum to one. This method computes all physical properties using a weighted average of the various phases according to their volume fractions within each control volume. The velocity components, shared by all phases, can only be found by solving a single set of momentum equations. Similarly, one energy equation is used to determine a standard temperature. Specifically, mass conservation is explained as follows [2]:

$$\nabla\left(\phi_q \rho_q \overrightarrow{V_q}\right) = 0 \tag{1}$$

where

$$\sum_{q=1}^{n} \phi_q = 1 \quad (2)$$

All properties are calculated as:

$$N = \sum_{q=1}^{n} \phi_q N_q (N \text{ is the number of phases}) \quad (3)$$

Furthermore, the equations for the conservation of momentum and energy are expressed as follows:

Momentum equation:

$$\nabla \cdot (\rho_m VV) = -\nabla p + \nabla \cdot (\mu_m \nabla V) \quad (4)$$

Energy equation:

$$\nabla \cdot \left(\rho_m V c_{pm} T\right) = \nabla \cdot (\lambda_m \nabla T) + Q \quad (5)$$

Q represents any internal heat generation from a chemical reaction, electrical heating, or another source.

For computing schemes used in our simulation, as the configuration settings used for a transient simulation, the timestep (Δt) was carefully selected to ensure that the Courant–Friedrichs–Lewy number maximum (CFL_{max}) ≤ 1. PISO (Pressure-Implicit with Splitting of Operators) is the Pressure-Velocity Coupling scheme used. Skewness correction and neighbor correction are set to 1, and skewness-neighbor coupling is activated. Pressure is handled with the PRESTO! (PREssure STaggering Option) scheme and momentum is discretized using the QUICK (Quadratic Upstream Interpolation for Convective Kinematics) method. The volume fraction is treated with a compressive scheme, and energy discretization employs the Third-Order MUSCL (Monotonic Upstream-Centered Scheme for Conservation Laws) method. The transient formulation used in this simulation is the Bounded Second Order Implicit scheme.

2.2 Grid Generation and Code Validation

Figure 1 illustrates the computational domain used for the simulation study, which is circular with a central wall circular cylinder surface subjected to a constant heat flux. The diameter of the cylinder is denoted by (D). The domain features an inlet labeled "velocity inlet," where the fluid enters, and an outlet marked as "pressure outlet," positioned directly opposite the inlet to facilitate fluid exit. The cylinder's diameter multiplied by 64 is the distance between the inlet and the outlet (64D). The boundary conditions comprise a velocity inlet, where the flow velocity is defined, and a pressure outlet, where the pressure is specified. This setup creates a controlled environment for analyzing the flow and heat transfer characteristics around the cylinder. By minimizing the influence of boundary effects on the flow field surrounding the cylinder, the large domain size relative to the cylinder diameter ensures accurate study results.

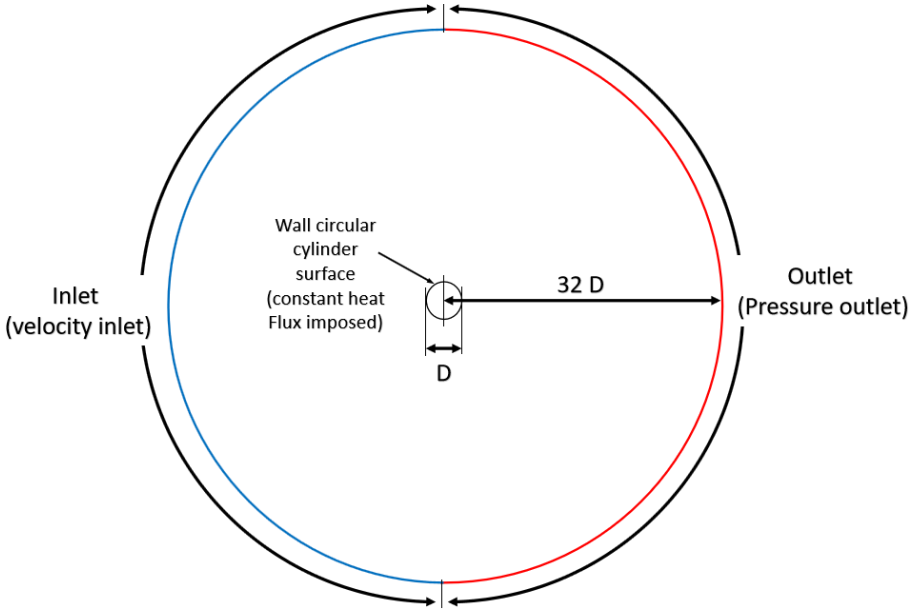

Fig. 1. Computational domain

Figure 2 shows the computational grid used for numerical simulations in full and close-up views. The grid is circular with dense node clustering at the center, gradually dispersing towards the edges. This design captures detailed phenomena near the center and optimizes computational resources by reducing resolution in outer areas.

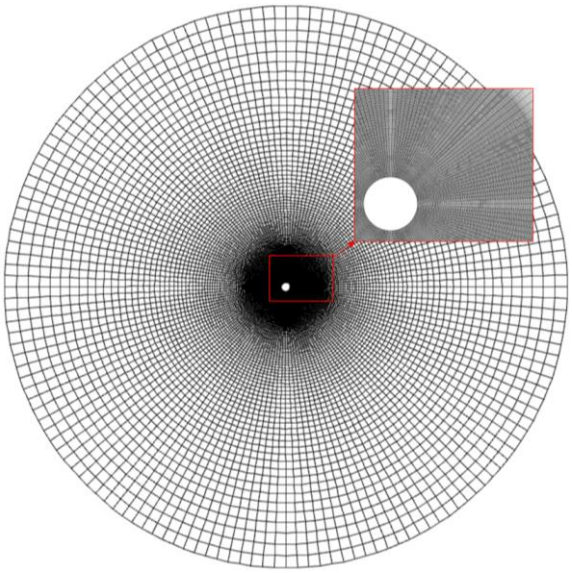

Fig. 2. A typical grid used for computations; full and close-up views

To make sure that the outcomes of the numerical simulation are independent of the grid size, Table 1 displays the grid independence test results. Seven different cases (M1 to M7) were analyzed with varying numbers of points around the cylinder (N_r) and corresponding mesh sizes. The parameters considered include the mean drag coefficient ($\bar{C}_D$), the fluctuation of drag coefficient ($\grave{C}_D$), the fluctuation of lift coefficient ($\grave{C}_L$), and Strouhal number (St).

The mean drag coefficient ($\bar{C}_D$) shows a slight variation initially, increasing from 1.319 in M1 to 1.334 in M3. Beyond M3, the value stabilizes at 1.333, indicating convergence from M4 onwards. The

fluctuation drag coefficient ($\grave{C}_D$) increases marginally from 5.4 × 10^{-3} in M1 to 6.4 × 10^{-3} in M2. From M3 to M7, ($\grave{C}_D$) stabilizes at 6.5 × 10^{-3}, suggesting grid independence from M3 onwards. The fluctuation lift coefficient ($\grave{C}_L$) increases from 0.210 in M1 to 0.230 in M3. After M3, ($\grave{C}_L$) remains constant at 0.230, indicating that sufficient grid resolution is achieved. The Strouhal number (St) starts at 0.1591 for M1 and gradually increases to 0.1641 by M3. From M4 onwards, (St) stabilizes at 0.1616, showing convergence.

Table 1
Results of grid independence test

Case	N_r	Mesh size × 10^3	$\bar{C}_D$	$\grave{C}_D$ × 10^{-3}	$\grave{C}_L$	St
M1	50	17.5	1.319	5.4	0.210	0.1591
M2	100	35	1.333	6.4	0.228	0.1641
M3	150	52.5	1.334	6.5	0.230	0.1641
M4	200	70	1.333	6.5	0.230	0.1616
M5	250	87.5	1.333	6.5	0.230	0.1616
M6	300	105	1.333	6.5	0.230	0.1616
M7	400	140	1.333	6.5	0.230	0.1591

The results demonstrate that mesh sizes greater than or equal to 52.5 × 10^3 (corresponding to case M3) provide consistent and stable values for all the key parameters ($\bar{C}_D$), ($\grave{C}_D$), ($\grave{C}_L$), and (St). Thus, a mesh size of 52.5 × 10^3 or higher is considered sufficient for grid independence in this simulation and for future simulations and analyses.

Table 2 compares the mean flow quantities for flow around a circular cylinder between various studies and the current study (case M3). The mean drag coefficient ($\bar{C}_D$) values range from 1.32 to 1.41 in the literature, and the present study reports a mean drag coefficient of 1.334, which falls within this range, indicating consistency with prior research. The fluctuation of drag coefficient ($\grave{C}_D$) reported in the literature are 6.3 × 10^{-3} and 6.4 × 10^{-3}, while the present study's value of 6.5 × 10^{-3} is slightly higher with 1.5% error. The fluctuation of lift coefficient ($\grave{C}_L$) values in the literature range from 0.2207 to 0.257, and the present study's value of 0.23013 aligns well with these values. The Strouhal number (St) values reported are between 0.164 and 0.172, with the present research noting a Strouhal number of 0.1641, which is consistent with literature values, suggesting accurate frequency prediction of vortex shedding. The comparison indicates that the results of the present study are consistent with those reported in previous literature for flow around a circular cylinder for Re=100. The slight variations observed are within acceptable ranges, and errors are lower than 1.5%.

Table 2
Validation of mean flow results on circular cylinder simulations at Re = 100

Author	$\bar{C}_D$	$\grave{C}_D$ × 10^{-3}	$\grave{C}_L$	St
Engelman and Jamnia [39]	1.405	-	-	0.172
Sharman *et al.,* [40]	1.33	6.4	0.230	0.164
Burbeau and Sagaut [41]	1.38	-	-	0.171
Muralidharan *et al.,* [42]	1.41	-	0.242	0.167
Posdziech and Grundmann [43]	1.31	-	-	0.163
Park *et al.,* [4]	1.33	-	-	0.165
Ali *et al.,* [44]	1.32	-	0.2207	0.164
Present study (M3)	1.334	6.5	0.230	0.164

Figure 3 illustrates the mean pressure coefficient ($\bar{C}_p$) distribution around a circular cylinder at a Reynolds number of 100. The present work shows a detailed pressure distribution profile that aligns closely with other works, indicating consistency and reliability in the current research methodology.

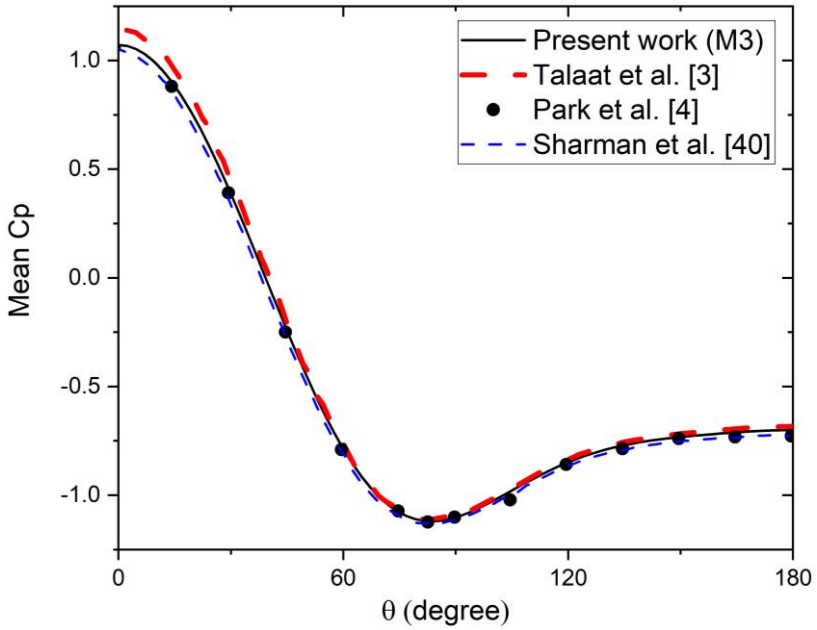

Fig. 3. Validation of mean pressure distribution over cylinder

At (θ = 0) degrees, all results show a peak of ($\bar{C}_p$) value around 1, expected due to the stagnation point at the front of the cylinder. A significant drop in ($\bar{C}_p$) is observed as (θ) increases, reaching a minimum around (θ = 80 to 100) degrees, indicative of flow separation and the formation of a wake region behind the cylinder. Post the minimum point, ($\bar{C}_p$) values gradually rise again towards (θ = 180) degrees. The overall shape and trend of the ($\bar{C}_p$) distribution is consistent with literature results. This figure demonstrates a strong agreement between the present work and previous studies by Abdelhamid *et al.,* [3], Park *et al.,* [4], and Sharman *et al.,* [40], validating the current results.

The distribution of a circular cylinder's mean Nusselt number $\overline{Nu}$ is shown in Figure 4. The time-averaged Nusselt number $\overline{Nu}$ is obtained by averaging the local Nusselt number over the time period of interest:

$$\overline{Nu} = \frac{1}{T}\int_0^T Nu(t)dt \tag{6}$$

Results of the current study are contrasted with those of Krall and Eckert [45] and Abdelhamid *et al.,* [3]. All three datasets show a high ($\overline{Nu}$) value at the front stagnation point (around ($\theta = 0°$)), which remains relatively high up to approximately ($\theta = 30°$), indicating strong convective heat transfer in this region. As (θ) increases from 30 to 90 degrees, there is a noticeable decline in ($\overline{Nu}$) for all datasets, with the present work maintaining slightly higher ($\overline{Nu}$) values compared to Abdelhamid *et al.,* [3] and Krall and Eckert [45]. Around ($\theta = 90°$), the midpoint of the cylinder, the Nusselt number reaches its minimum, with the present work showing the lowest minimum, suggesting reduced convective heat transfer efficiency at this point.

Beyond ($\theta = 90°$), ($\overline{Nu}$) begins to increase again. The present work shows a slightly sharper recovery than the other datasets, reaching a higher ($\overline{Nu}$) at ($\theta = 180°$), indicating enhanced heat transfer in the rear half of the cylinder. The results from the present work are consistent with those from Abdelhamid *et al.,* [3] and Krall and Eckert [45], demonstrating a similar overall distribution in ($\overline{Nu}$). This comparative analysis reveals that all studies agree on the general behavior of ($\overline{Nu}$) around the cylinder.

Figure 4 effectively illustrates the distribution of the mean Nusselt number around a circular cylinder. The present work aligns well with previous studies.

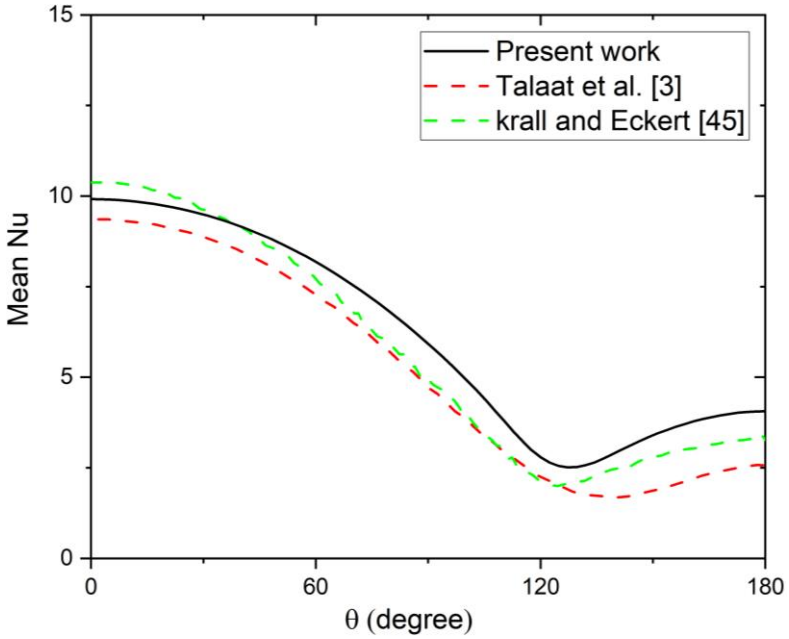

Fig. 4. Mean Nusselt number distribution over cylinder

3. Results and Discussion

The flow analysis results that include the nanoparticle presence are described in detail in this section. The percentage value of the volume fraction (Φ) indicates the concentration of nanoparticles. In our study, we varied the volume fraction (Φ) from 1% to 10% in increments of 1%. Table 3 presents the thermophysical characteristics of the research materials used in this study, namely water as the base fluid and Al_2O_3 as nanoparticles:

Table 3
Water's thermophysical characteristics and nanoparticles

Physical properties	Fluid (H_2O)	Al_2O_3
Cp, J/kg K	4179	765
ρ, kg/m^3	997.1	3970
λ, W/mK	0.613	40
β × 10^{-5}, 1/K	21	0.85

Figure 5 shows the fluctuating drag coefficient $(\grave{C}_D)$ and the mean drag coefficient $(\bar{C}_D)$ against volume fraction (Φ) ranging from 0% to 10%, illustrating that the mean drag coefficient steadily increases with volume fraction, from approximately 1.33 at (Φ = 0%) to around 1.7 at (Φ = 10%). Similarly, the fluctuation in the drag coefficient rises from approximately 6.5 × 10^{-3} at (Φ = 0%) to about 1.8 × 10^{-2} at (Φ = 10%). This suggests that the drag force on the cylinder increases with the volume fraction, and the drag coefficient's mean and fluctuating components positively correlate with it. The steady increase in the mean drag coefficient with increasing nanoparticle volume fractions is attributed to increased momentum diffusion, as nanoparticles enhance the fluid's effective viscosity, leading to more excellent resistance to flow and higher drag on the cylinder. This occurs because the particles disrupt the smooth passage of the fluid around the cylinder, generating larger boundary layers and stronger shear forces.

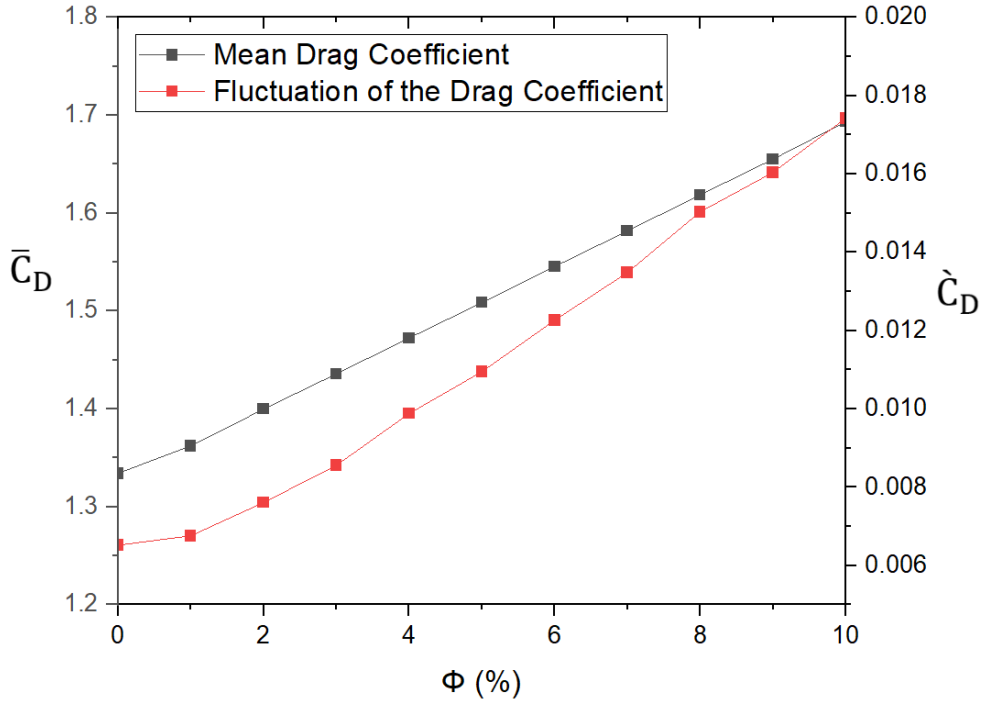

Fig. 5. Mean and fluctuation of drag coefficient for Φ=1%-10%

The variation between the Strouhal number (St) and the fluctuation of the lift coefficient $(\grave{C}_L)$ with volume fraction (Φ), as illustrated in Figure 6, shows that both increase as the volume fraction rises. Specifically, the Strouhal number starts at around 0.164 for (Φ = 0%) and gradually increases to approximately 0.175 at (Φ = 10%). In comparison, the fluctuation of the lift coefficient begins at about 0.23 for (Φ = 0%) and rises significantly to around 0.36 at (Φ = 10%). This indicates that the frequency of vortex shedding, represented by the Strouhal number, increases with higher volume fractions, suggesting that the flow becomes more unstable as the nanoparticle concentration rises. The increase in the Strouhal number with (Φ) implies higher vortex shedding frequencies, as the interaction between the particles and the base fluid leads to faster vortex detachment. The enhanced thermal conductivity and viscosity of nanofluids contribute to quicker energy dissipation in the wake, promoting earlier and more frequent vortex shedding.

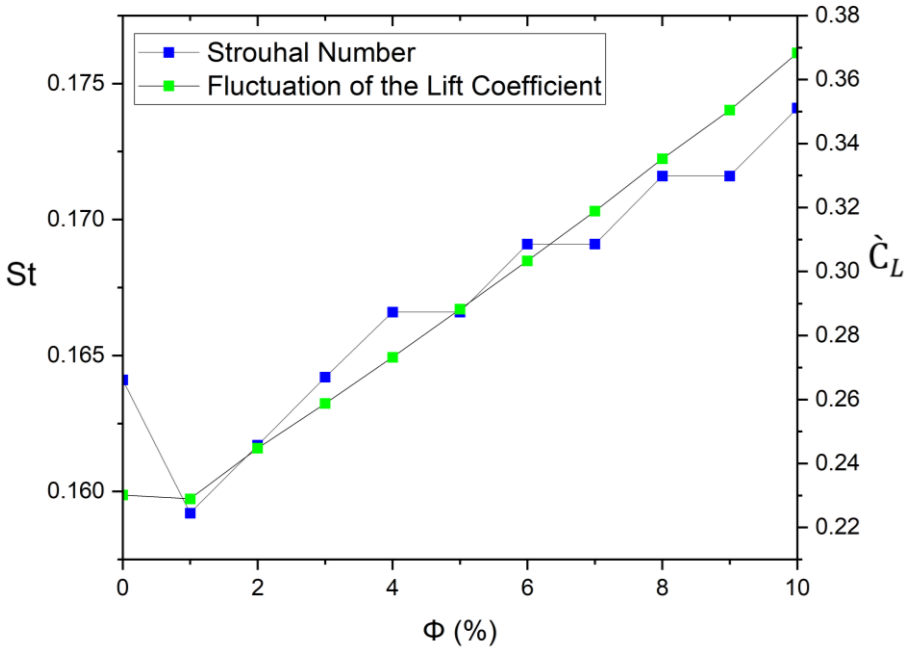

Fig. 6. Strouhal number and lift coefficient for Φ=1%-10%

Figure 7 and Figure 8 depict the mean pressure distribution $(\bar{C}_p)$ over a circular cylinder for different nanofluid volume fractions (Φ). Figure 7 shows the mean pressure distribution for (Φ) values ranging from 1% to 5%, while Figure 8 presents the mean distribution for (Φ) values ranging from 5% to 10%. Both figures exhibit a similar trend: $(\bar{C}_p)$ starts at a maximum at the stagnation point (θ = 0°), decreases sharply near (θ = 80°), then gradually increases toward the rear stagnation point (θ = 180°). As (Φ) increases, it noticeably affects the pressure distribution over the cylinder. For (Φ=10%), the $(\bar{C}_p)$ at (θ = 30°) is relatively high, indicating a strong pressure gradient, but as (Φ) increases, $(\bar{C}_p)$ at this angle slightly decreases, suggesting that nanoparticles influence the flow characteristics, smoothing the gradient and reducing local pressure. At (θ = 180°), higher (Φ) results in less negative $(\bar{C}_p)$, indicating a reduction in the adverse pressure gradient. The differences in $(\bar{C}_p)$ become more pronounced at higher (Φ) values, mainly between 6% and 10%, as seen in Figure 8, compared to the range from 1% to 5% in Figure 7. This variation suggests changes in the boundary layer characteristics and separation points on the cylinder surface. The smoother pressure gradients observed with increasing nanoparticle concentrations indicate a modification in boundary layer behavior. Nanoparticles enhance the fluid's thermal conductivity, promoting faster heat dissipation from the cylinder surface, resulting in a thinner thermal boundary layer that delays flow separation and shifts wake formation downstream. Consequently, the adverse pressure gradient behind the cylinder decreases, reducing flow separation and vortex intensity, with changes in the separation point and wake structure playing a key role in determining the drag and lift forces on the cylinder.

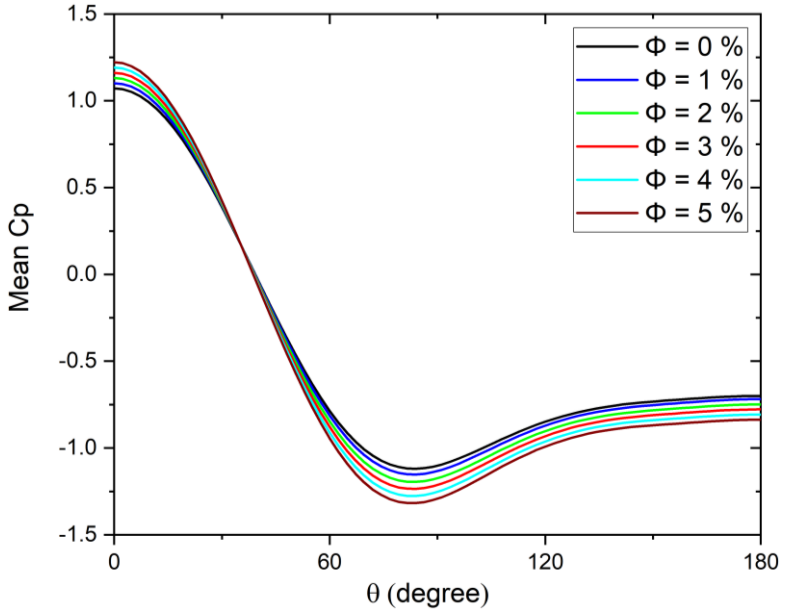

Fig. 7. Mean pressure distribution over circular cylinder for Φ= 1% - 5%

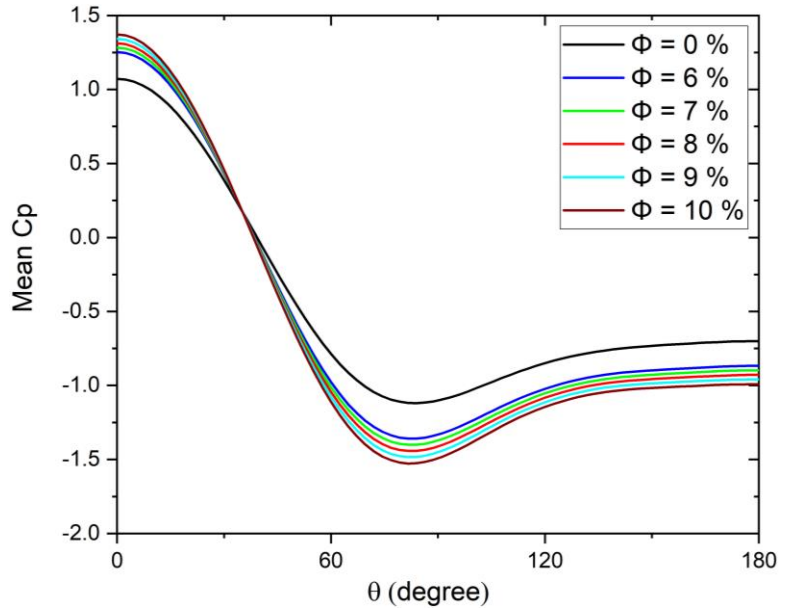

Fig. 8. Mean pressure distribution over a circular cylinder for Φ= 6% - 10%

Figure 9 and Figure 10 illustrate the averaged local Nusselt number $(\overline{Nu})$ distributions over a circular cylinder for different volume fractions of nanoparticles (Φ), providing insight into the heat transfer characteristics around the cylinder with varying nanoparticle concentrations. Figure 9 shows the time-averaged local Nusselt number over a circular cylinder for volume fractions, ranging from $(\Phi = 1\%)$ to $(\Phi = 5\%)$, with the local Nusselt number plotted on the cylinder surface. Key observations from Figure 9 include an increase in the time-averaged local Nusselt number with higher nanoparticle concentrations, with the highest time-averaged local Nusselt number at $(\theta = 0°)$ decreasing along the cylinder's surface, and the lowest Nusselt number corresponding to $(\Phi = 0\%)$ (pure fluid), indicating reduced heat transfer compared to nanofluids. The local Nusselt number's behavior reflects the enhanced heat transfer due to the presence of nanoparticles, where the higher

thermal conductivity of nanofluids leads to a more efficient transfer of heat from the cylinder surface to the surrounding fluid. This results in higher heat transfer rates at the front stagnation point and a more uniform temperature distribution around the cylinder. Physically, the presence of nanoparticles increases the fluid's capacity to absorb and transport heat, reducing the thermal boundary layer thickness and leading to a significant increase in the Nusselt number as (Φ) increases, with the improvement in heat transfer being most important at the front stagnation point and progressively decreasing along the surface of the cylinder.

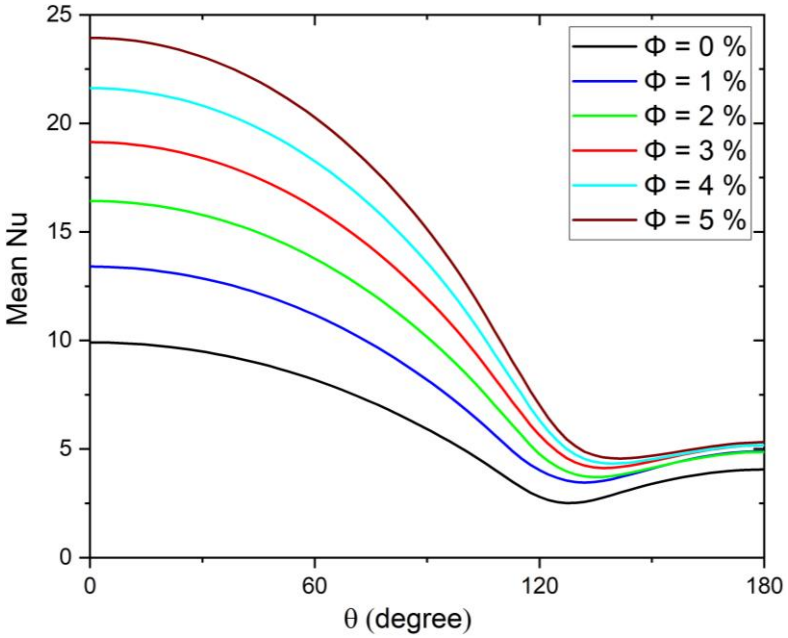

Fig. 9. Time-averaged local Nusselt number over circular cylinder for Φ=1%-5%

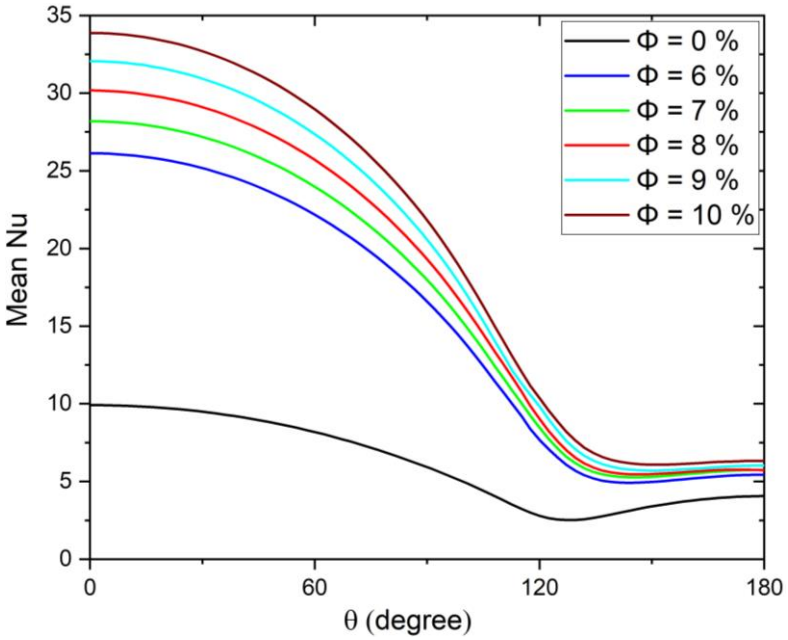

Fig. 10. Time-averaged local Nusselt number over circular cylinder for Φ=6%-10%

Figure 11 illustrates the time-averaged volume fraction of the second phase (nanofluid) for various (Φ) values.

At low (Φ) values (1% to 3%), the flow field shows minor disturbances, with a relatively low and uniform distribution of the second phase in the wake region.

As (Φ) increases from 4% to 6%, more pronounced disturbances appear, and the wake behind the cylinder displays an asymmetric distribution of the second phase.

At higher (Φ) values (7% to 8%), the presence of nanoparticles becomes more pronounced in the region where vortex formation and shedding processes are visible, and the interaction between the phases intensifies, indicating four axisymmetric areas in the wake of the cylinder.

A thin, strongly concentrated nanofluid layer is observed for (Φ = 9% and 10%). In this layer, flow separation occurs at the separation angle on both the upper and lower surfaces, subsequently adhering to the rear of the cylinder.

Physically, the asymmetry in nanoparticle distribution in the wake region at higher concentrations can be explained by the interaction between nanoparticles and the fluid, which creates complex flow structures and leads to non-uniform dispersion in the wake.

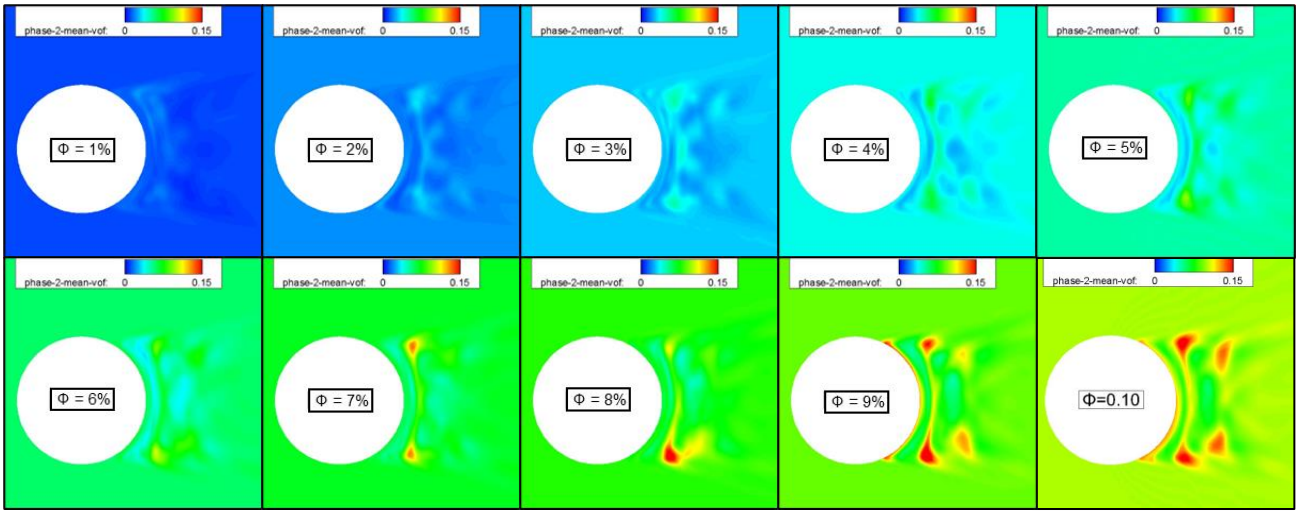

Fig. 11. Contours of time-averaged volume fraction of the second phase (nanofluid)

Figure 12 illustrates the contours of time-averaged temperature in the near-wake region, showing that as the nanoparticle concentration increases from 1% to 10%, there are noticeable changes in the wake structure and temperature distribution. Lower (Φ) values result in an extended and distinct wake. In comparison, higher (Φ) values lead to a more compact wake, indicating stronger thermal diffusion and improved heat transfer due to the enhanced thermal conductivity of the nanofluid. The compact wake and uniform temperature distribution observed at higher nanoparticle concentrations indicate stronger thermal mixing in the wake, driven by the nanofluid's improved conductive properties. As (Φ) increases, the temperature distribution becomes more uniform, suggesting improved thermal diffusion and a thinner thermal boundary layer near the cylinder surface. This leads to enhanced heat transfer at the solid-fluid interface. Overall, the figure demonstrates that higher nanoparticle concentrations enhance heat transfer efficiency, as evidenced by more uniform temperature distributions and reduced thermal gradients in the wake.

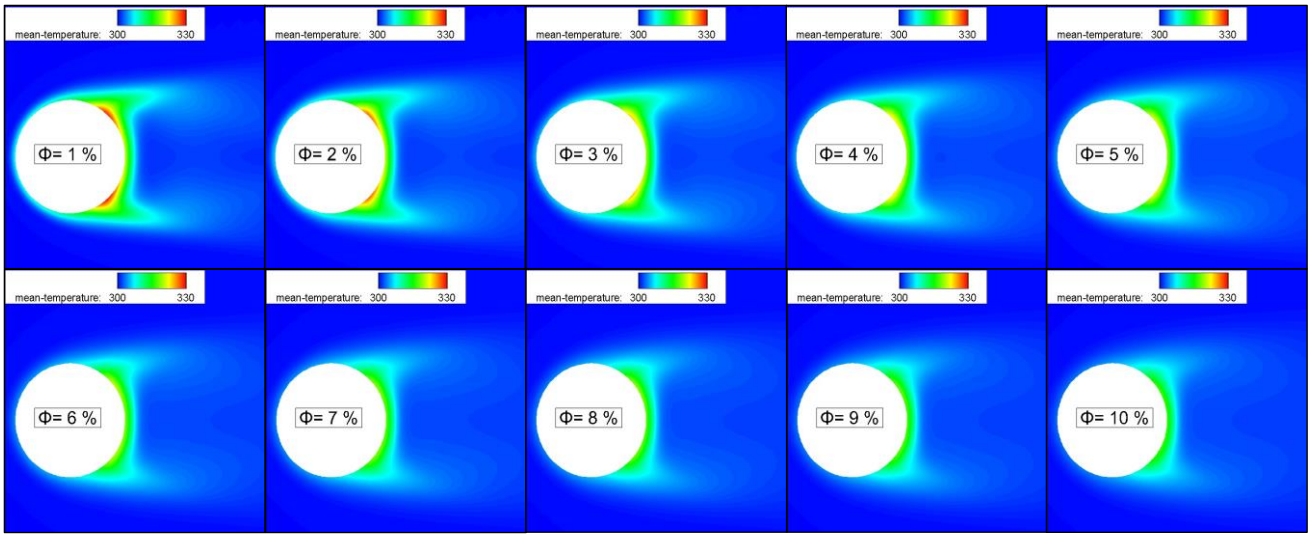

Fig. 12. Contours of time-averaged temperature in near wake region for Φ=1%-10%

4. Conclusions

A nanofluid flow and heat transfer around a heated circular cylinder were successfully modeled and examined in this work. Heat transfer characteristics around the circular cylinder were significantly enhanced by adding nanofluids, more precisely, those with different volume fractions. The volume of fluid (VOF) model was used in the numerical simulations, demonstrating good agreement with experimental and benchmark data. The mesh independence tests confirmed that a mesh size of 52.5 x 10^3 nodes or higher provides consistent and accurate results, establishing the reliability of the computational model employed in this study. The results demonstrated that higher nanoparticle concentrations lead to increased Nusselt numbers, indicating enhanced heat transfer rates due to the superior thermal properties of nanofluids compared to traditional fluids. Additionally, the study revealed that the mean and fluctuating components of the drag coefficient (C_D) and lift coefficient (C_L) increase with the volume fraction (Φ). At a 10% volume fraction, the mean drag coefficient rose from approximately 1.33 to 1.7. In contrast, the lift coefficient's fluctuation increased from 0.23 to 0.36, implying that higher nanoparticle concentrations result in greater aerodynamic forces acting on the cylinder. Besides, the frequency of vortex shedding, represented by the Strouhal number (St), was also influenced by the nanoparticle volume fraction, increasing from 0.164 at 0% volume fraction to 0.175 at 10%, indicating more frequent vortex shedding with higher nanoparticle concentrations. This behavior suggests a direct relationship between nanoparticle concentration and the dynamic stability of the flow. The mean pressure distribution ($\bar{C}_p$) around the cylinder revealed notable changes with varying volume fractions of nanofluids, with higher nanoparticle concentrations smoothing the pressure gradient, reducing the local pressure at specific angles, and altering the adverse pressure gradient at the rear stagnation point. The study provides significant insight into the complex interaction between fluid flow and nanoparticles, demonstrating the effectiveness of the (VOF) model for capturing the intricate flow dynamics. Notably, higher nanoparticle concentrations led to more frequent vortex shedding, an observation that could have implications for optimizing heat transfer devices in various engineering applications.

In future studies, extending the investigation across a wider range of Reynolds numbers would be beneficial. By including lower and higher values, the flow characteristics under different regimes—from laminar to turbulent—could be better understood, offering more comprehensive insights into how nanofluids behave in various flow conditions. Additionally, exploring different nanofluid

compositions, such as CuO, TiO_2, or carbon-based nanomaterials, would provide a comparative thermal performance analysis, helping to identify which combinations of nanoparticles and base fluids offer the most significant heat transfer enhancement. Beyond just varying the composition, future studies should consider the effects of nanoparticle shape and size, as these parameters can substantially influence flow dynamics and heat transfer efficiency. Furthermore, integrating flow control techniques, such as vortex generators or active flow mechanisms like suction and blowing, could reduce drag and increase heat transfer rates. These control methods could optimize the interaction between the nanofluid and the circular cylinder, paving the way for more efficient thermal management systems in engineering applications.

References

[1] Safaei, Mohammad Reza, AminHossein Jahanbin, Ali Kianifar, Samira Gharehkhani, Akeel Shebeeb Kherbeet, Marjan Goodarzi, and Mahidzal Dahari. "Mathematical modeling for nanofluids simulation: a review of the latest works." *Modeling and Simulation in Engineering Sciences* (2016): 189-220. https://doi.org/10.5772/64154

[2] Naphon, Paisarn, and Lursukd Nakharintr. "Turbulent two phase approach model for the nanofluids heat transfer analysis flowing through the minichannel heat sinks." *International Journal of Heat and Mass Transfer* 82 (2015): 388-395. https://doi.org/10.1016/j.ijheatmasstransfer.2014.11.024

[3] Abdelhamid, Talaat, Md Mahbub Alam, and Md Islam. "Heat transfer and flow around cylinder: Effect of corner radius and Reynolds number." *International Journal of Heat and Mass Transfer* 171 (2021): 121105. https://doi.org/10.1016/j.ijheatmasstransfer.2021.121105

[4] Park, Jeongyoung, Kiyoung Kwon, and Haecheon Choi. "Numerical solutions of flow past a circular cylinder at Reynolds numbers up to 160." *KSME International Journal* 12 (1998): 1200-1205. https://doi.org/10.1007/BF02942594

[5] Nashee, Sarah Rabee, and Haiyder Minin Hmood. "Numerical study of heat transfer and fluid flow over circular cylinders in 2D cross flow." *Journal of Advanced Research in Applied Sciences and Engineering Technology* 30, no. 2 (2023): 216-224. https://doi.org/10.37934/araset.30.2.216224

[6] Bhattacharyya, Suvanjan, Supratim Das, Anubhab Sarkar, Anindya Guin, and Ayan Mullick. "Numerical simulation of flow and heat transfer around hexagonal cylinder." *International Journal of Heat and Technology* 35, no. 2 (2017): 360-363. https://doi.org/10.18280/ijht.350218

[7] Aun, Tan S., Mohd Z. Abdullah, and Prem Gunnasegaran. "Influence of low concentration of diamond water nanofluid in loop heat pipe." *International Journal of Heat and Technology* 35, no. 3 (2017): 539-548. https://doi.org/10.18280/ijht.350310

[8] Majdi, Hasan S., Ammar Abdulkadhim, and Azher M. Abed. "Computational Fluid Dynamics Investigation of Buoyancy Driven Flow Between Circular Body and Wavy Enclosure Filled with Nanofluid/Porous Medium." *International Journal of Heat & Technology* 38, no. 2 (2020). https://doi.org/10.18280/ijht.380216

[9] Ahmed, Shayekh, Amzad Hossain, Md Zahangir Hossain, and Md Mamun Molla. "Forced convection of non-Newtonian nanofluid in a sinusoidal wavy channel with response surface analysis and sensitivity test." *Results in Engineering* 19 (2023): 101360. https://doi.org/10.1016/j.rineng.2023.101360

[10] Hossain, Amzad, and Md Mamun Molla. "MHD mixed convection of non-Newtonian power-law ferrofluid in a wavy enclosure." *Journal of Thermal Analysis and Calorimetry* 148, no. 21 (2023): 11871-11892. https://doi.org/10.1007/s10973-023-12485-7

[11] Hossain, Amzad, Md Mamun Molla, Md Kamrujjaman, Muhammad Mohebujjaman, and Suvash C. Saha. "MHD mixed convection of non-Newtonian Bingham nanofluid in a wavy enclosure with temperature-dependent thermophysical properties: a sensitivity analysis by response surface methodology." *Energies* 16, no. 11 (2023): 4408. https://doi.org/10.3390/en16114408

[12] Afsana, Sadia, Md Mamun Molla, Preetom Nag, Litan Kumar Saha, and Sadia Siddiqa. "MHD natural convection and entropy generation of non-Newtonian ferrofluid in a wavy enclosure." *International Journal of Mechanical Sciences* 198 (2021): 106350. https://doi.org/10.1016/j.ijmecsci.2021.106350

[13] Nag, Preetom, and Md Mamun Molla. "Double-diffusive natural convection of non-Newtonian nanofluid considering thermal dispersion of nanoparticles in a vertical wavy enclosure." *AIP Advances* 11, no. 9 (2021). https://doi.org/10.1063/5.0058405

[14] Korib, Kamel, Nabila Ihaddadene, Rafik Bouakkaz, and Yacine Khelili. "Numerical simulation of forced convection of nanofluid around a circular cylinder." *Archives of Thermodynamics* (2019): 3-16.

[15] Mahat, Rahimah, Muhammad Saqib, Imran Ulah, Sharidan Shafie, and Sharena Mohamad Isa. "Magnetohydrodynamics Mixed Convection of Viscoelastic Nanofluid Past a Circular Cylinder with Constant Heat Flux." *CFD Letters* 14, no. 9 (2022): 52-59. https://doi.org/10.37934/cfdl.14.9.5259

[16] Farooq, M., Aisha Anjum, Sadique Rehman, and M. Y. Malik. "Entropy analysis in thermally stratified Powell-Eyring magnesium-blood nanofluid convection past a stretching surface." *International Communications in Heat and Mass Transfer* 138 (2022): 106375. https://doi.org/10.1016/j.icheatmasstransfer.2022.106375

[17] Farooq, Aamir, Sadique Rehman, Abdulaziz N. Alharbi, Muhammad Kamran, Thongchai Botmart, and Ilyas Khan. "Closed-form solution of oscillating Maxwell nano-fluid with heat and mass transfer." *Scientific Reports* 12, no. 1 (2022): 12205. https://doi.org/10.1038/s41598-022-16503-w

[18] Hussain, Syed M., Rujda Parveen, Nek Muhammad Katbar, Sadique Rehman, Assmaa Abd-Elmonem, Nesreen Sirelkhtam Elmki Abdalla, Hijaz Ahmad et al. "Entropy generation analysis of MHD convection flow of hybrid nanofluid in a wavy enclosure with heat generation and thermal radiation." *Reviews on Advanced Materials Science* 63, no. 1 (2024): 20240037. https://doi.org/10.1515/rams-2024-0037

[19] Lin, Yuanjian, Sadique Rehman, Nevzat Akkurt, Tim Shedd, Muhammad Kamran, Muhammad Imran Qureshi, Thongchai Botmart, Abdulaziz N. Alharbi, Aamir Farooq, and Ilyas Khan. "Free convective trickling over a porous medium of fractional nanofluid with MHD and heat source/sink." *Scientific Reports* 12, no. 1 (2022): 20778. https://doi.org/10.1038/s41598-022-25063-y

[20] Algehyne, Ebrahem A., Fahad Maqbul Alamrani, Showkat Ahmad Lone, Zehba Raizah, Sadique Rehman, and Anwar Saeed. "Homotopy assessment on the stratified micropolar Carreau-Yasuda bio-inspired radiative copper and gold/blood nanofluid flow on a Riga plate." *Journal of Thermal Analysis and Calorimetry* (2024): 1-16. https://doi.org/10.1007/s10973-024-13072-0

[21] Raza, Haider, Sohail Farooq, Sobia Sattar, Sadique Rehman, Aamir Farooq, Muhammad Kamran, Mansoor Alshehri, and Nehad Ali Shah. "Melting phenomenon of thermally stratified MHD Powell-Eyring nanofluid with variable porosity past a stretching Riga plate." *Reviews on Advanced Materials Science* 63, no. 1 (2024): 20240020. https://doi.org/10.1515/rams-2024-0020

[22] Ashraf, Muhammad, and Zia Ullah. "Effects of variable density on oscillatory flow around a non-conducting horizontal circular cylinder." *AIP Advances* 10, no. 1 (2020). https://doi.org/10.1063/1.5127967

[23] Ashraf, Muhammad, Asifa Ilyas, Zia Ullah, and Amir Abbas. "Periodic magnetohydrodynamic mixed convection flow along a cone embedded in a porous medium with variable surface temperature." *Annals of Nuclear Energy* 175 (2022): 109218. https://doi.org/10.1016/j.anucene.2022.109218

[24] Ashraf, Muhammad, Zia Ullah, Saqib Zia, Sayer O. Alharbi, Dumitru Baleanu, and Ilyas Khan. "Analysis of the Physical Behavior of the Periodic Mixed-Convection Flow around a Nonconducting Horizontal Circular Cylinder Embedded in a Porous Medium." *Journal of Mathematics* 2021, no. 1 (2021): 8839146. https://doi.org/10.1155/2021/8839146

[25] Ullah, Zia, Muhammad Bilal, Ioannis E. Sarris, and Abid Hussanan. "MHD and thermal slip effects on viscous fluid over symmetrically vertical heated plate in porous medium: keller box analysis." *Symmetry* 14, no. 11 (2022): 2421. https://doi.org/10.3390/sym14112421

[26] Ullah, Zia, Nevzat Akkurt, Haifaa F. Alrihieli, Sayed M. Eldin, Aisha M. Alqahtani, Abid Hussanan, Muhammad Ashraf, and Mah Jabeen. "Temperature-dependent density and magnetohydrodynamic effects on mixed convective heat transfer along magnetized heated plate in thermally stratified medium using Keller box simulation." *Applied Sciences* 12, no. 22 (2022): 11461. https://doi.org/10.3390/app122211461

[27] Idrees, Muhammad, Zia Ullah, Jihad Younis, Sohail Ahmad, and Hafeez Ahmad. "Stabilization of Double Inverted Pendulum Systems Based on Hierarchical Sliding Mode Control Techniques." *Mathematical Problems in Engineering* 2023, no. 1 (2023): 3916279. https://doi.org/10.1155/2023/3916279

[28] Boudjemline, Attia, Zia Ullah, Musaad S. Aldhabani, Hammad Al-Shammari, Essam R. El-Zahar, Laila F. Seddek, and Ahmed Alamer. "Amplitude and oscillating frequency of chemically reactive flow along inclined gravity-driven surface in the presence of thermal conductivity." *Case Studies in Thermal Engineering* 54 (2024): 104001. https://doi.org/10.1016/j.csite.2024.104001

[29] Ullah, Zia, Hammad Alotaibi, Ayesha Akhter, Ilyas Khan, and Shafiullah Niazai. "Computational analysis of thermal performance of temperature dependent density and Arrhenius-activation energy of chemically reacting nanofluid along polymer porous sheet in high temperature differences." *AIP Advances* 14, no. 6 (2024). https://doi.org/10.1063/5.0213991

[30] Alqahtani, Bader, Essam R. El-Zahar, Muhammad Bilal Riaz, Laila F. Seddek, Asifa Ilyas, Zia Ullah, and Ali Akgül. "Computational analysis of microgravity and viscous dissipation impact on periodical heat transfer of MHD fluid along porous radiative surface with thermal slip effects." *Case Studies in Thermal Engineering* (2024): 104641. https://doi.org/10.1016/j.csite.2024.104641

[31] Ullah, Zia, Essam R. El-Zahar, Laila F. Seddek, Aboulbaba Eladeb, Lioua Kolsi, Abdulrhman M. Alsharari, Jihad Asad, and Ali Akgül. "Microgravity analysis of periodic oscillations of heat and mass transfer of Darcy-Forchheimer

nanofluid along radiating stretching surface with Joule heating effects." *Results in Physics* (2024): 107810. https://doi.org/10.1016/j.rinp.2024.107810

[32] Al Arni, Saleh, Atef El Jery, Zia Ullah, M. D. Alsulami, Essam R. El-Zahar, Laila F. Seddek, and Nidhal Ben Khedher. "Oscillatory and non-oscillatory analysis of heat and mass transfer of Darcian MHD flow of nanofluid along inclined radiating plate with joule heating and multiple slip effects: Microgravity analysis." *Case Studies in Thermal Engineering* (2024): 104681. https://doi.org/10.1016/j.csite.2024.104681

[33] Ullah, Zia, Mohamed Ahmed Said, M. D. Alsulami, Saleh Al Arni, Nidal HE Eljaneid, Ali Hakami, and Nidhal Ben Khedher. "Thermal radiation and soret/dufour effects on amplitude and oscillating frequency of darcian mixed convective heat and mass rate of nanofluid along porous plate." *Case Studies in Thermal Engineering* 59 (2024): 104562. https://doi.org/10.1016/j.csite.2024.104562

[34] Ullah, Zia, Essam R. El-Zahar, Laila F. Seddek, Nidhal Becheikh, Badr M. Alshammari, Musaad S. Aldhabani, and Lioua Kolsi. "Solar radiation and heat sink impact on fluctuating mixed convective flow and heat rate of Darcian nanofluid: Applications in electronic cooling systems." *Case Studies in Thermal Engineering* 59 (2024): 104592. https://doi.org/10.1016/j.csite.2024.104592

[35] Nabwey, Hossam A., Muhammad Ashraf, Zia Ullah, A. M. Rashad, and Ali J. Chamkha. "A comprehensive review on the dynamical behavior of heat and fluid flow mechanism: thermal performance across different geometries." *Partial Differential Equations in Applied Mathematics* (2024): 100808. https://doi.org/10.1016/j.padiff.2024.100808

[36] Almheidat, Maalee, Zia Ullah, Mohamed Ahmed Said, Mohamed Hussien, Saleh Al Arni, M. D. Alsulami, Ahmed Osman Ibrahim, and Abdullah A. Faqihi. "Turbulent and non-turbulent analysis of thermomagnetic convection and heat transfer of darcian radiative nanofluid flow across inclined stretching surface in microgravity environment." *Case Studies in Thermal Engineering* 60 (2024): 104812. https://doi.org/10.1016/j.csite.2024.104812

[37] Nabwey, Hossam A., Zia Ullah, Asifa Ilyas, Muhammad Ashraf, Ahmed M. Rashad, Sumayyah I. Alshber, and Miad Abu Hawsah. "Reduced Gravity and Magnetohydrodynamic Effects on Transient Mixed Convection Flow Past a Magnetized Heated Cone Embedded in Porous Medium." *Journal of Mathematics* 2023, no. 1 (2023): 9618432. https://doi.org/10.1155/2023/9618432

[38] Urmi, Wajiha Tasnim, Md Mustafizur Rahman, Kumaran Kadirgama, Zetty Akhtar Abd Malek, and Wahaizad Safiei. "A comprehensive review on thermal conductivity and viscosity of nanofluids." *Journal of Advanced Research in Fluid Mechanics and Thermal Sciences* 91, no. 2 (2022): 15-40. https://doi.org/10.37934/arfmts.91.2.1540

[39] Engelman, Michael S., and Mohammad-Ali Jamnia. "Transient flow past a circular cylinder: a benchmark solution." *International Journal for Numerical Methods in Fluids* 11, no. 7 (1990): 985-1000. https://doi.org/10.1002/fld.1650110706

[40] Sharman, Bryce, Fu-Sang Lien, Lars Davidson, and Christoffer Norberg. "Numerical predictions of low Reynolds number flows over two tandem circular cylinders." *International Journal for Numerical Methods in Fluids* 47, no. 5 (2005): 423-447. https://doi.org/10.1002/fld.812

[41] Burbeau, A., and P. Sagaut. "Simulation of a viscous compressible flow past a circular cylinder with high-order discontinuous Galerkin methods." *Computers & Fluids* 31, no. 8 (2002): 867-889. https://doi.org/10.1016/S0045-7930(01)00055-X

[42] Muralidharan, K., Sridhar Muddada, and B. S. V. Patnaik. "Numerical simulation of vortex induced vibrations and its control by suction and blowing." *Applied Mathematical Modelling* 37, no. 1-2 (2013): 284-307. https://doi.org/10.1016/j.apm.2012.02.028

[43] Posdziech, O., and R. Grundmann. "A systematic approach to the numerical calculation of fundamental quantities of the two-dimensional flow over a circular cylinder." *Journal of Fluids and Structures* 23, no. 3 (2007): 479-499. https://doi.org/10.1016/j.jfluidstructs.2006.09.004

[44] Ali, Ussama, M. D. Islam, and Isam Janajreh. "Flow over rotationally oscillating heated circular cylinder at low Reynolds number." *Ocean Engineering* 265 (2022): 112515. https://doi.org/10.1016/j.oceaneng.2022.112515

[45] Krall, K. M., and E. R. G. Eckert. "Heat transfer to a transverse circular cylinder at low Reynolds numbers including rarefaction effects." In *International Heat Transfer Conference Digital Library*. Begel House Inc., 1970. https://doi.org/10.1615/IHTC4.2380